Compressibility stripes for mesoscopic quantum Hall samples

C. Sohrmann and R.A. Römer

Department of Physics and Centre for Scientific Computing, University of Warwick, Gibbet Hill Road, Coventry CV4 7AL, UK

E-mail: `c.sohrmann@warwick.ac.uk, r.roemer@warwick.ac.uk`

Abstract. We numerically investigate the interplay of disorder and electron-electron interactions in the integer quantum Hall effect. In particular, we focus on the behaviour of the electronic compressibility as a function of magnetic field and electron density. We find manifestations of non-linear screening and charging effects around integer filling factors, consistent with recent imaging experiments. Our calculations exhibit g-factor enhancement as well as strong overscreening in the centre of the Landau bands. Even though the critical behaviour appears mostly unaffected by interactions, important implications for the phase diagram arise. Our results are in very good agreement with the experimental findings and strongly support the relevance of electron-electron interactions for understanding integer quantum Hall physics.

1. Introduction

The *integer* quantum Hall effect (IQHE) — observed in two-dimensional electron systems (2DES) subject to a strong perpendicular magnetic field [1] — has been well explained based on single-particle arguments [2–11]. Crossing the centre of each disorder-broadened Landau level, the Hall conductivity σ_{xy} jumps by e^2/h and the longitudinal conductivity σ_{xx} is finite. The accompanying localization-delocalization transition is governed by a critical exponent $\tilde{\nu} = 2.34 \pm 0.04$ [12,13], a universal quantity independent of microscopic details of electron motion, the disorder realization, and thus the chosen material. In fact, it is precisely this astonishing resilience of the quantum Hall (QH) effect that makes it an ideal metrological standard [14].

However, recent experiments on mesoscopic MOSFET devices have questioned the validity of such a simple single-particle picture. Measurements of the Hall conductance as a function of magnetic field B and gate voltage [15] exhibited regular patterns along integer filling factors. It was argued that these patterns should be attributed to Coulomb blockade effects. Similar patterns have been found recently also in measurements of the electronic compressibility κ as a function of B and electron density n_{e} in the IQHE [16] as well as the fractional quantum Hall effect (FQHE) [17]. From these measurements it turns out that deep in the localized regime between two Landau levels, stripes of constant width with particularly small κ can be identified. These stripes consist of a collection of small-κ lines, identifiable with localized states, and their number is independent of B. This is inconsistent with a single-particle picture where one expects a fan-diagram of lines emanating from $(0, 0)$ in the (B, n_{e})-plane. The authors argue that their results may be explained qualitatively by non-linear screening of the impurity charge density at the Landau level band edges. Clearly such screening effects — explained within a Thomas-Fermi approach [16] — are beyond a simple non-interacting theory. This immediately raises a question on the status of the aforementioned universality of the QH transition [15, 18, 19], which was obtained largely within a single-particle approach [9, 12, 20–25]. Further qualitative support for the screening arguments where recently given in [26,27], where a Hartree-Fock (HF) approach lead to a non-fan structure for κ in the (B, n_{e}) diagram; a further Thomas-Fermi-type investigation showed that charging lines with the desired slopes can indeed be found within a simple model for the impurity potentials [28].

In the present paper, we quantitatively investigate the effects of Coulomb interactions on the compressibility in the (B, n_{e})-plane within a HF approach. HF accounts for Thomas-Fermi screening effects while at the same time leading to a critical exponent ν whose value is consistent with the results of the non-interacting approaches [29,30]. We find that the observed charging lines in the compressibility can be well reproduced and that the width of each group of lines is well estimated by a force balance argument. Thus we can quantitatively explain the lines and stripes in the compressibility as a function of (B, n_{e}). We note that these results fully support the qualitative picture proposed in [16, 26–28].

2. Formulation of the QH model in Landau basis

In order to model a high-mobility heterostructure in the QH regime, we consider a 2DES in the (x, y)-plane subject to a perpendicular magnetic field $\vec{B} = B\vec{e}_z$. The system can be described by a Hamiltonian of the form

$$H^\sigma_{2\mathrm{DES}} = h^\sigma + V_\mathrm{C} = \frac{(\vec{p} - e\vec{A})^2}{2m^*} + \frac{\sigma g^* \mu_\mathrm{B} B}{2} + V_\mathrm{I}(\vec{r}) + V_\mathrm{C}(\vec{r}, \vec{r}'), \tag{1}$$

where $\sigma = \pm 1$ is a spin degree of freedom, V_I is a smooth random potential modeling the effect of the electron-impurity interaction, V_C represents the electron-electron interaction term and m^*, g^*, and μ_B are the effective electron mass, g-factor, and Bohr magneton, respectively. In order to avoid edge effects we impose a torus geometry of size $L \times L$ onto the system [31]. The electron-impurity interaction is modeled by an electrostatic potential due to a remote impurity density separated from the plane of the 2DES by a spacer-layer of thickness d, as found for instance in modulation-doped GaAs-GaAlAs heterojunctions. Within the plane of the 2DES, this creates a random, spatially correlated potential with a typical length scale d. We use N_I Gaussian-type "impurities", randomly distributed at $\vec{r}_s$, with random strengths $w_s \in [-W, W]$, and a fixed width d, such that $V_\mathrm{I}(\vec{r}) = \sum_{s=1}^{N_\mathrm{I}} (w_s/\pi d^2) \exp[-(\vec{r} - \vec{r}_s)^2/d^2] = \sum_{\vec{q}} V_\mathrm{I}(\vec{q}) \exp(i\vec{q} \cdot \vec{r})$ with

$$V_\mathrm{I}(\vec{q}) = \sum_{s=1}^{N_\mathrm{I}} \frac{w_s}{L^2} \exp\left(-\frac{d^2 |\vec{q}|^2}{4} - i\vec{q} \cdot \vec{r}_s\right), \tag{2}$$

where $q_{x,y} = 2\pi j/L$ and $j = -N_\phi, -N_\phi - 1, \ldots, N_\phi$. The areal density of impurities therefore is given by $n_\mathrm{I} = N_\mathrm{I}/L^2$. The limit $d \to 0$ yields a potential of δ-type that would be more adequate for modeling low-mobility structures. We will highlight a few differences between the two cases in the following sections. The electron-electron interaction potential has the form $V_\mathrm{C}(\vec{r}, \vec{r}') = \gamma e^2/4\pi\epsilon\epsilon_0 |\vec{r} - \vec{r}'| = \sum_{\vec{q}} V_\mathrm{C}(\vec{q}) \exp[i\vec{q} \cdot (\vec{r} - \vec{r}')]$, with

$$V_\mathrm{C}(\vec{q}) = \frac{\gamma e^2}{4\pi\epsilon\epsilon_0 l_\mathrm{c}} \frac{1}{N_\phi |\vec{q}| l_\mathrm{c}}. \tag{3}$$

The parameter γ will allow us to continually adjust the interaction strength; $\gamma = 1$ corresponds to the bare Coulomb interaction. Choosing the vector potential in Landau gauge, $\vec{A} = Bx\vec{e}_y$, the kinetic part of the Hamiltonian is diagonal in the Landau functions [32]

$$\varphi_{n,k}(\vec{r}) = \frac{1}{\sqrt{2^n n! \sqrt{\pi} l_\mathrm{c} L}} \exp\left[iky - \frac{(x - kl_\mathrm{c}^2)^2}{2l_\mathrm{c}^2}\right] H_n\left(\frac{x - kl_\mathrm{c}^2}{l_\mathrm{c}}\right), \tag{4}$$

where n labels the Landau level index, $k = 2\pi j/L$ with $j = 0, \ldots, N_\phi - 1$ labels the momentum, $H_n(x)$ is the nth Hermite polynomial, and $l_\mathrm{c} = \sqrt{\hbar/eB}$ the magnetic length. These functions are extended and L-periodic in y-direction and localized in x direction. For the system's many-body state, $|\Phi\rangle$, we use the usual ansatz [33, 34] of an anti-symmetrized product of single particle wave-functions $\psi^\sigma_\alpha(\vec{r})$ (Slater determinant), which

we choose as a linear combination of Landau states

$$\psi_\alpha^\sigma(\vec{r}) = \sum_{n=0}^{N_{\mathrm{LL}}-1} \sum_{k=0}^{N_\phi-1} \vec{C}_{n,k}^{\alpha,\sigma} \chi_{n,k}(\vec{r}), \tag{5}$$

with N_{LL} being the number of Landau levels and the periodic Landau functions

$$\chi_{n,k}(\vec{r}) = \langle \vec{r} | nk \rangle = \sum_{j=-\infty}^{\infty} \varphi_{n,k+jL/l_{\mathrm{c}}^2}(\vec{r}), \tag{6}$$

in order to meet the boundary conditions. The number of flux quanta piercing the 2DES of size $L \times L$ is given by $N_\phi = L^2/2\pi l_{\mathrm{c}}^2$, yielding a total number of $M = N_{\mathrm{LL}}N_\phi$ states per spin direction. The filling of the system is characterized by the filling factor $\nu = N_{\mathrm{e}}/N_\phi$, with N_{e} being the number of electrons in the system and areal density $n_{\mathrm{e}} = N_{\mathrm{e}}/L^2$. The total Landau level density is given by $n_0 = eB/h$.

3. Hartree-Fock equation in the Landau basis and its numerical solution

We are left with finding the correct expansion coefficients $\vec{C}_{n,k}^{\alpha,\sigma}$ [33–36]. The Hamiltonian is represented in matrix form using the periodic Landau states $|nk\rangle$ and we have

$$\begin{aligned}
\mathbf{H}_{n,k;n',k'}^\sigma &= \langle nk | H_{\mathrm{2DES}}^\sigma | n'k' \rangle \\
&= \left(n + \frac{1}{2} + \frac{\sigma g^*}{4} \frac{m^*}{m_{\mathrm{e}}} \right) \hbar\omega_{\mathrm{c}} \delta_{n,n'} \delta_{k,k'} + \mathbf{V}_{n,k;n',k'} + \mathbf{F}_{n,k;n',k'}^\sigma \quad , \tag{7}
\end{aligned}$$

with the cyclotron energy $\hbar\omega_{\mathrm{c}} = \hbar eB/m^*$. The disorder matrix elements are given by $\mathbf{V}_{n,k;n',k'} = \sum_{\vec{q}} V_{\mathrm{I}}(\vec{q}) S_{n,k;n',k'}(\vec{q})$, where mixing of Landau levels is included. The explicit form of the plane wave matrix elements $S_{n,k;n',k'}(\vec{q}) = \langle nk | \exp(i\vec{q} \cdot \vec{r}) | n'k' \rangle$ is computed in the Appendix. The elements of the Fock matrix $\mathbf{F}$ are

$$\mathbf{F}_{n,k;n',k'}^\sigma = \sum_{\sigma'} \sum_{l,m,l',m'} \left(G_{n,k;n',k'}^{m,l;m',l'} - \delta_{\sigma,\sigma'} G_{n,k;m',l'}^{m,l;n',k'} \right) \mathbf{D}_{m,l;m',l'}^{\sigma'} \quad , \tag{8}$$

where the first term is the Hartree and the second the Fock contribution. The bielectronic integrals $G_{n,k;n',k'}^{m,l;m',l'} = \sum_{\vec{q}\neq 0} V_{\mathrm{C}}(\vec{q}) S_{n,k;n',k'}(\vec{q}) S_{m,l;m',l'}(-\vec{q})$ can be further simplified as given in the Appendix. A homogeneous, positive background is assumed that neutralizes the charge of the electrons and thereby prevents the Coulomb term from diverging as $|\vec{q}| \to 0$. In fact, this interaction with the background can be shown to cancel with the term $|\vec{q}| = 0$ in $\mathbf{F}$ up to a contribution of the order of L^{-1} due to the finite system size [37]. The density matrix is given by

$$\mathbf{D}_{m,l;m',l'}^\sigma = \sum_{\alpha=1}^{M} f(\epsilon_\alpha^\sigma) \left(\mathbf{C}_{m,l}^{\alpha\sigma} \right)^* \mathbf{C}_{m',l'}^{\alpha,\sigma} \quad , \tag{9}$$

with $\mathrm{Tr}(\mathbf{D}) = N_{\mathrm{e}}$ and $\mathbf{D}^\sigma \mathbf{D}^\sigma = \mathbf{D}^\sigma$. Here $f(\epsilon)$ denotes the Fermi function. The total energy E_{tot} in terms of the above matrices is given as

$$E_{\mathrm{tot}} = \mathrm{Tr}(\mathbf{hD} + \frac{1}{2}\mathbf{FD}) = \frac{1}{2} \sum_\sigma \sum_{n,k;n',k'} \left(2\mathbf{h}_{n,k;n',k'}^\sigma + \mathbf{F}_{n,k;n',k'}^\sigma \right) \mathbf{D}_{n,k;n',k'}^\sigma . \tag{10}$$

A variational minimization of $\langle\Psi|H_{2\text{DES}}|\Psi\rangle$ with respect to the coefficients yields the Hartree-Fock-Roothaan equation [38], a self-consistent eigenvalue problem which in compact form can be written as

$$\mathbf{H}^\sigma\mathbf{C}^\sigma = \mathbf{C}^\sigma\mathbf{E}^\sigma, \tag{11}$$

with $\mathbf{C}^\sigma = (\vec{C}_1^\sigma, \ldots, \vec{C}_M^\sigma)$ being the matrix of eigenvectors and $\mathbf{E}^\sigma = \text{diag}(\epsilon_1^\sigma, ..., \epsilon_M^\sigma)$ the diagonal matrix of the eigenvalues $\epsilon_1^\sigma \leq \epsilon_2^\sigma \leq \ldots \leq \epsilon_M^\sigma$ [39].

Following the aufbau principle [40], the density matrix is constructed starting from the energetically lowest lying state up to the Fermi level ϵ_F. In our calculations, we keep N_e fixed and compute ϵ_F as the energy of the highest occupied state afterwards. Since the Fock matrix depends on the density matrix, which in turn depends on the full solution of problem, (11) has to be calculated self-consistently which is numerically quite challenging. In the first step we use the solution of the non-interacting Hamiltonian $\mathbf{h}^\sigma = \langle nk|h^\sigma|n'k'\rangle$ as a starting guess for the coefficients $\mathbf{C}^\sigma$. From this solution, $\mathbf{C}^{(0)}$, we construct the density and Fock matrices and finally the full Hamiltonian. Diagonalization yields an improved solution, $\mathbf{C}^{(1)}$. The process continues until convergence of the density matrix has been achieved. In practice, we compute the norm of the difference between successive density matrices $||\mathbf{D}^{(n+1)} - \mathbf{D}^{(n)}|| < \varepsilon$. Here $||\cdot||$ denotes the Hilbert-Schmidt norm defined as $||\mathbf{A}|| = \text{Tr}(\mathbf{A}\mathbf{A}^*)^{1/2}$.

However, convergence of this Roothaan algorithm [38] is not always assured. Especially for fillings close to zero or an integer value it may run into an oscillating limit cycle. Subtracting a small multiple of the density matrix, $b\mathbf{D}^\sigma$, from the Hamiltonian $\mathbf{H}^\sigma = \mathbf{h}^\sigma + \mathbf{F}^\sigma$ favours already occupied states, thereby suppressing such oscillations. The eigenvalues shift by $\epsilon_i^\sigma \rightarrow \epsilon_i^\sigma - b \quad \forall \quad \epsilon_i^\sigma \leq \epsilon_\text{F}$, but eigenstates are not affected. This algorithm is known as the level shifting algorithm [41] and b is the level-shift parameter. We choose $b \approx 1.76e^2/L$ which is exactly the contribution of the neglected $V_\text{C}(\vec{q}=0)$ term that does not cancel with the background charge due to the finite system size. This prevents the occupied and unoccupied states from mixing and stabilizes the convergence of the algorithm, although at the cost of slower convergence. A further improvement of convergence is achieved by constructing the new density matrix $\mathbf{D}^{(n+1)}$ as a mixture of the updated and the previous one, i.e. $\tilde{\mathbf{D}}^{(n+1)} = \lambda\mathbf{D}^{(n+1)} + (1-\lambda)\mathbf{D}^{(n)}$, with $\lambda \in [0,1]$. We adjust λ in each step automatically such that the fastest global convergence is guaranteed [40].

In each HF step, assembling the dense Fock matrix $\mathbf{F}^\sigma$ scales as $\mathcal{O}(N_\text{LL}^4 N_\phi^3)$ and is clearly very time-consuming. An improved scheme, even though generally possible, is of little advantage since the diagonalization is of similar complexity. For the calculation of a particular disorder configuration and magnetic field, a self-consistent run has to be made for each of the M possible filling factors. Hence, the complexity of a complete HF calculation is of the order $\mathcal{O}(2KN_\text{LL}^5 N_\phi^4)$ with K the number of iterations until convergence. The dependence on the system size is therefore $\mathcal{O}(L^8)$. For system sizes of $L \sim 300\text{nm}$, we find $K \sim 100 - 1000$. In all results present here, convergence of the HF scheme is assumed for $\varepsilon \leq 10^{-6}$.

4. Chemical potential and electronic compressibility

The electronic compressibility $\kappa = (\partial n_e/\partial\mu)/n_e^2$ reflects the ability of the 2DES to absorb electrons when changing the chemical potential. With $\mu = \partial E_{tot}/\partial N_e$, we find $\partial\mu/\partial n_e = L^2(\partial^2 E_{tot}/\partial N_e^2)$. Hence, for finite sample calculations, we can obtain κ from $E_{tot}(N_e)$ using

$$\frac{\partial\mu}{\partial n_e} \approx L^2 \left[E_{tot}(N_e + 1) - 2E_{tot}(N_e) + E_{tot}(N_e - 1) \right]. \tag{12}$$

Alternatively, at $T = 0$, we can compute the change in the chemical potential for N_e electrons by noting that the Fermi energy $\epsilon_F(N_e) = \mu(N_e)$. Thus we immediately have

$$\frac{\partial\mu}{\partial n_e} = L^2 \left[\epsilon_F(N + 1) - \epsilon_F(N) \right]. \tag{13}$$

This turns out to be numerically more stable than (10) and shall be used in the following.

When the Fermi energy lies in a region of highly localized states, it takes a considerable energy to accommodate another electron, and thus the compressibility is low. On the other hand, in a region of delocalized states a newly added electron is much more easily absorbed and κ is high. For a non-interacting system, κ is proportional to the tunneling density of states (DOS) [42] and expected to exhibit a fan-like structure in the (B, n_e) diagram. In particular, the resonances in κ need not align with slopes equal to integer filling factors [43]. In the interacting case, κ is proportional to the thermodynamic density of states (TDOS) and the inverse screening length. We note that experimentally the change of the chemical potential is detected when changing the back gate voltage and hence the electron density at constant B [16, 17].

5. Sample mobility and DOS

In order to tune our parameters for the electron-impurity interaction to the experiment, we estimate the zero field mobility, defined as $\mu_0 = e\tau/m^*$, with τ being the transport scattering time [42, 44]. For a short-range δ-impurity potential, τ is identical to the single-particle momentum relaxation time, τ_s, which determines the level broadening, $(\Gamma/2)^2 = \hbar\omega_c\hbar/2\pi\tau_s$ [45]. For long-range potential, however, these two times can be very different [46] and knowledge about the level broadening does not necessarily imply knowledge about the mobility and vice versa. In fact, for a smooth potential with $d \gg l_c$ we have $(\Gamma/2)^2 = \left\langle [V_I(\vec{r}) - \langle V_I(\vec{r})\rangle_{\vec{r}}]^2 \right\rangle_{\vec{r}}$, which does not depend on B. In that case, we can determine the mobility from the transport cross-section calculated in Born approximation [32, 45]. Since the transport scattering time is momentum dependent, we take the low temperature limit, where the relevant scattering time is the one for electrons having Fermi momentum $k_F = (2\pi n_e)^{1/2}$. With a radially symmetric electron-impurity interaction potential (for a single scatterer), $u(\vec{r})$, we obtain for the transport scattering time

$$\tau^{-1} = \frac{n_I m^*}{2\pi\hbar^3} \int_0^{2\pi} d\theta \left[1 - \cos(\theta) \right] \left| \tilde{u}(2k_F \sin(\theta/2)) \right|^2, \tag{14}$$

with the Fourier transform $u(\vec{k}) = \int d^2\vec{r} u(\vec{r}) \exp(-i\vec{r} \cdot \vec{k})$ and $\tilde{u}(k) = u(|\vec{k}|)$. In case of δ-interaction and uniformly distributed strengths, we simply have $\tilde{u}(k) = W/\sqrt{3}$ and the $\cos(\theta)$ term in (14) vanishes. Without it, (14) becomes the expression for τ_s, which proves the equivalence of τ and τ_s for short-range potentials. For long-range potentials, however, forward (small θ) scattering receives little weight since it hardly impairs the electron movement and $\tau/\tau_\mathrm{s} \gg 1$. In order to model a situation comparable to the experiments of [16], we use material parameters for GaAs ($g^* = -0.44$ for the effective g-factor, $m^* = 0.067 m_\mathrm{e}$ for the effective mass) and impurity parameters of $W/\mathrm{nm}^2 \simeq 4\mathrm{eV}$ with a concentration of $n_\mathrm{I} = 3.2 \cdot 10^{11} \mathrm{cm}^{-2}$ (e.g. $N_\mathrm{I} = 288$ for $L = 300\mathrm{nm}$ or $N_\mathrm{I} = 392$ for $L = 350\mathrm{nm}$). Assuming $n_\mathrm{e} \approx n_\mathrm{I}$, for the δ-potential this yields a mobility of $\mu_0 \simeq 10^3 \mathrm{cm}^2/\mathrm{Vs}$, whereas for $d = 40\mathrm{nm}$ ($\approx$ spacer layer thickness) we get $\mu_0 \simeq 10^6 \mathrm{cm}^2/\mathrm{Vs}$ — a value which is reasonable for a high mobility sample such as a GaAs-GaAlAs heterojunction.

We have calculated the DOS in the lowest Landau level by averaging over at least 1000 samples in the non-interacting and the interacting system. In Figure 1 we show results for Gaussian and δ-impurities for three system sizes $L = 400, 500$, and 600nm for the non-interacting case as well as the interacting case. Within the accuracy of the calculation, we find the DOS to be independent of the system size, irrespective of interactions, as of course expected for our static disorder model [47]. Furthermore, in the interacting case, we find a strong suppression of the DOS at the Fermi level. The formation of this Coulomb gap and its non-criticality has been studied previously [29, 30, 37, 48]. In case of Gaussian-type impurities we also observe a strong reduction of the band broadening due to screening of the impurity potential, while the bandwidth in systems with δ-type impurities is hardly affected by interactions.

6. Scaling of the participation ratio

The participation ratio P_α is defined as the inverse of the variance of the charge density in the state α,

$$P_\alpha = \left(L^2 \int d^2\vec{r} |\psi_\alpha(\vec{r})|^4 \right)^{-1} . \tag{15}$$

Large values of P_α correspond to spatially extended states, while low values indicate a confined state [49, 50]. This is intuitively understood by the fact that the density of an extended state varies much less over space than a highly localized one. Thus P_α is a measure of the degree of localization [51] and may be computed in our model as

$$P_\alpha = \frac{l_\mathrm{c}^2}{L^2} \sum_{\substack{n,n',m,m' \\ k,k',l,l'}} \sum_{\vec{q}} (\mathbf{C}_{n,k}^\alpha)^* \mathbf{C}_{n',k'}^\alpha (\mathbf{C}_{m,l}^\alpha)^* \mathbf{C}_{m',l'}^\alpha S_{n,k;n',k'}(\vec{q}) S_{m,l;m',l'}(-\vec{q}). \tag{16}$$

It has been shown that unscreened HF-interactions do not alter the critical exponent $\tilde{\nu}$ while renormalizing the dynamical scaling exponent to $z = 1$ [29, 30, 53]. As a check to our HF results, we calculate P_α of spinless electrons in the lowest Landau level for

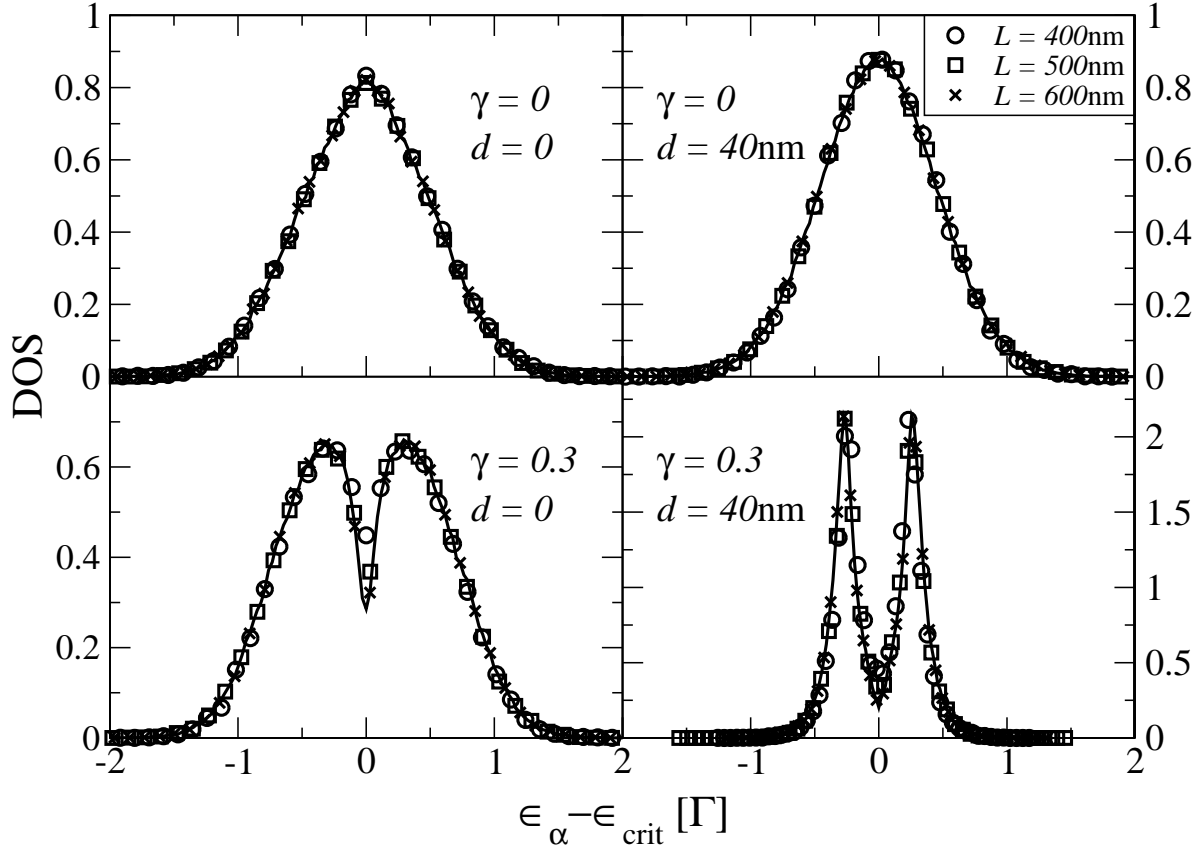**Figure 1.** DOS at $B = 3$T for the lowest Landau level in a non-interacting (top row, $\gamma = 0$) and a HF-interacting (bottom row, $\gamma = 0.3$ at $\nu = 1/2$) QH system for 3 system sizes. The left column shows results for δ-type impurities ($d = 0$) with $W/\text{nm}^2 = 2$eV, the right column corresponds to Gaussian-type impurities with $d = 40$nm and $W/\text{nm}^2 = 4$eV ($W/d^2 = 2.5$meV). The results in all cases are averaged over at least 1000 samples. Error bars are less than the symbol sizes. Note the strong Coulomb reduction of the DOS at the critical energy ($\epsilon_\alpha = \epsilon_{\text{crit}}$) in the interacting systems.

the same samples as in Section 5. The participation ratio is expected to obey the single parameter scaling form [54]

$$P_\alpha = L^{D(2)-2}\Pi\left(L^{1/\tilde{\nu}}|\epsilon_\alpha - \epsilon_{\text{crit}}|\right), \tag{17}$$

with the anomalous diffusion coefficient $D(2) \approx 1.6$ — related to the multifractal character of the critical states [55–57] — and the critical exponent $\tilde{\nu} \approx 2.3$ [12]. Figure 2 shows the scaling function for the non-interacting and an interacting system at filling factor $\nu = 1/2$. The scaling function collapses reasonably well onto a single curve for both, non-interacting and HF-interacting systems. We find $D(2) = 1.62 \pm 0.10$ as typical average over both, HF- and non-interacting systems as shown in Figure 3. This demonstrates the irrelevance of interactions and the type of disorder for the multifractal dimension of the critical state, in very good agreement with previous results [27, 30, 57]. A similar fit in the tails of P_α is numerically less accurate but still yields estimates for $\tilde{\nu}$ between 2 and 2.4, compatible with the expected value 2.34 ± 0.04 [12, 23].
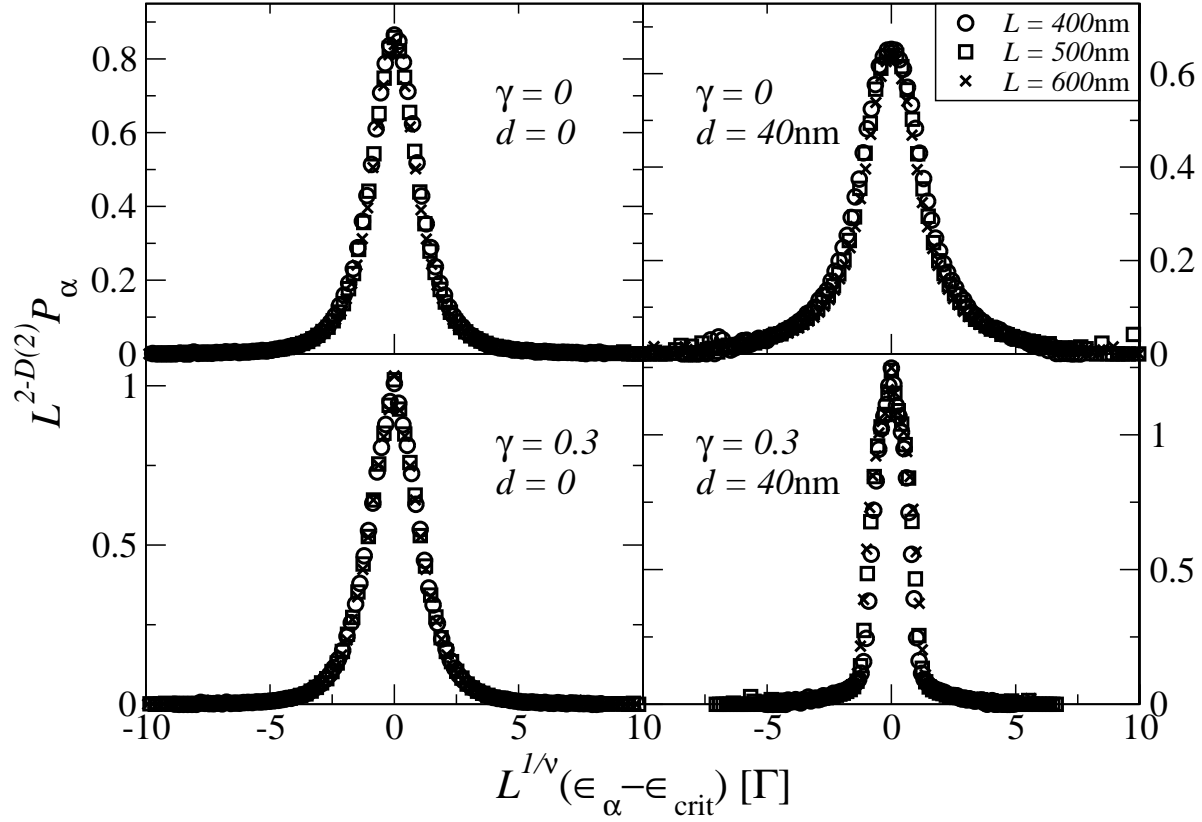
Figure 2. Scaling functions of the participation ratio P_α at $B = 3\text{T}$ for the non-interacting (top row, $\gamma = 0$) and the HF-interacting (bottom row, $\gamma = 0.3$ at $\nu = 1/2$) systems averaged over at least 1000 samples and using $D(2) = 1.62$, $\tilde{\nu} = 2.34$. The left column shows results for δ-type impurities ($d = 0$), the right column corresponds to Gaussian-type impurities with $d = 40\text{nm}$. Values for L have been scaled by the magnetic length. Fluctuations in the tails are due to a smaller number of data points.

7. Charging lines and stripes in the electronic compressibility

Let us first briefly recall the experimental results of [16,17] most relevant to the present investigation. The compressibilities in the (B, n_e)-plane (i) exhibit only little variation in regions close to the QH transitions at half-integer filling factors, but (ii) show a strong variation between Landau bands at integer fillings which by virtue of the relation $n_e = \nu e B/h$ correspond to lines of constant slope. Furthermore, (iii) these regions of strong variation seem to have a width which is B and Landau level index independent and (iv) within these stripes, thin lines of equal slope jeB/h, $j = 0, 1, \ldots$ can be identified. In what follows, we have calculated the electronic compressibility as outlined in Section 4 in the lowest two, spin-split Landau levels for a sample of size $L = 300\text{nm}$ at magnetic fields between $B = 0.2\text{T}$ and $B = 6\text{T}$.
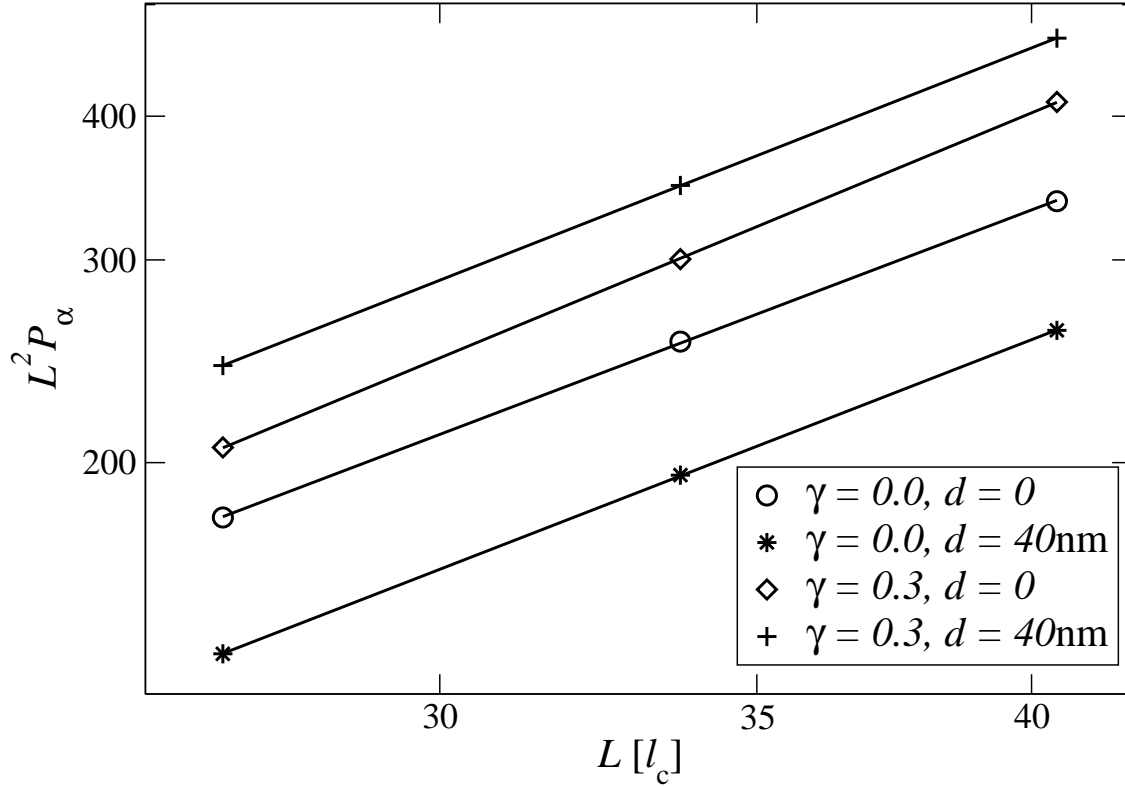
Figure 3. Power-law fit of the system size dependence of P_α at $B = 3$T according to (17) for non-interacting and HF-interacting systems around $\epsilon_\alpha = \epsilon_{\text{crit}}$. $\circ$ and $\diamond$ denote δ-type impurities ($d = 0$) whereas $*$ and $+$ show results for Gaussian-type impurities with $d = 40$nm. The error bars for the data points are smaller than the symbol sizes. The $D(2)$ values are 1.57 ± 0.2 ($\gamma = 0$, $d = 0$), 1.6 ± 0.1 ($\gamma = 0$, $d = 40$nm), 1.7 ± 0.1 ($\gamma = 0.3$, $d = 0$), 1.62 ± 0.05 ($\gamma = 0.3$, $d = 40$nm). Values for L are scaled by the magnetic length.

7.1. Compressibilities for the non-interacting system

Figure 4 shows our results for the *inverse* compressibility κ^{-1} of non-interacting ($\gamma = 0$) electrons in the two lowest orbital Landau levels, including spin. Darker areas in the plot reflect states of higher compressibility, hence a more delocalized regime. Lighter areas are more strongly localized states. Due to the weak Zeemann splitting, we do not observe the two spin bands separately. Rather, both bands remain nearly degenerate and lie almost on top of each other. Hence, we only find a single, very strongly incompressible region between the first and the second orbital Landau level at $\nu = 2$. This broad line is due to the band gap and the highly localized states at the band edges. Other less pronounced lines are visible along different filling factors, seemingly mostly emanating from $(0, 0)$. Some lines even appear to have a varying slope as shown in the inset of Figure 4. We interpret these features as the aforementioned fingerprints of scattering resonances in the disorder potential [43] which do not necessarily need to align with constant filling factors. Moreover, we clearly observe an increasing number of those lines with increasing magnetic field. At $\nu = 0$ and 4, the compressibility is again low.
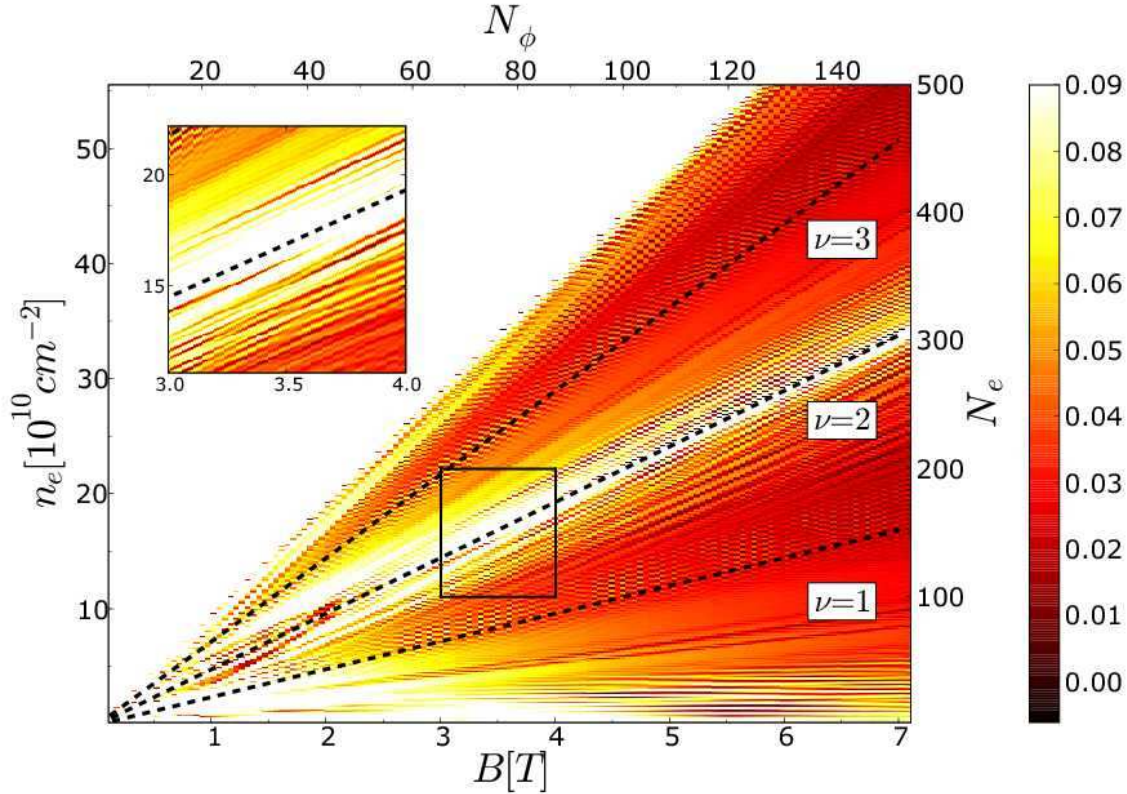
Figure 4. Inverse electronic compressibility κ^{-1} for a non-interacting system of size $L = 300$nm with disorder strength $W/d^2 = 2.5$meV in the (B, n_e)-plane. The color scale spans two standard deviations around the average of κ^{-1}. The inset shows more detailed results for the region marked by a black rectangle.

7.2. Effects of the Hartree-Fock interaction

We next include interaction with $\gamma = 0.3$. This is not yet the full $\gamma = 1$ Coulomb term, but the results are numerically more stable while at the same time not being dramatically different from $\gamma = 1$. Furthermore, $\gamma < 1$ is essentially equivalent to increased disorder with the full Coulomb interaction present.

Figures 5, 6, and 7 show results in the (B, n_e)-plane for an interacting system of size $L = 300$nm with disorder strengths $W/d^2 = 1.25, 2.5$, and 3.75meV, respectively, at fixed impurity range $d = 40$nm. We observe that the exchange interaction results in an effective g-factor substantially enhanced from its bare value [58–60], leading to a clear separation of the two spin bands. This yields two additional strongly incompressible stripes at $\nu = 1$ and $\nu = 3$, indicated by particularly high κ^{-1} values. Quite different from the non-interacting case, we find that most of the incompressible lines form groups which align parallel in the (B, n_e)-plane along integer filling factors. Above a certain minimal magnetic field, the width of these groups — the number of the lines — is independent of the magnetic field and Landau level, forming *incompressible* stripes of constant width around integer filling factors. Overall, this behaviour is strikingly similar
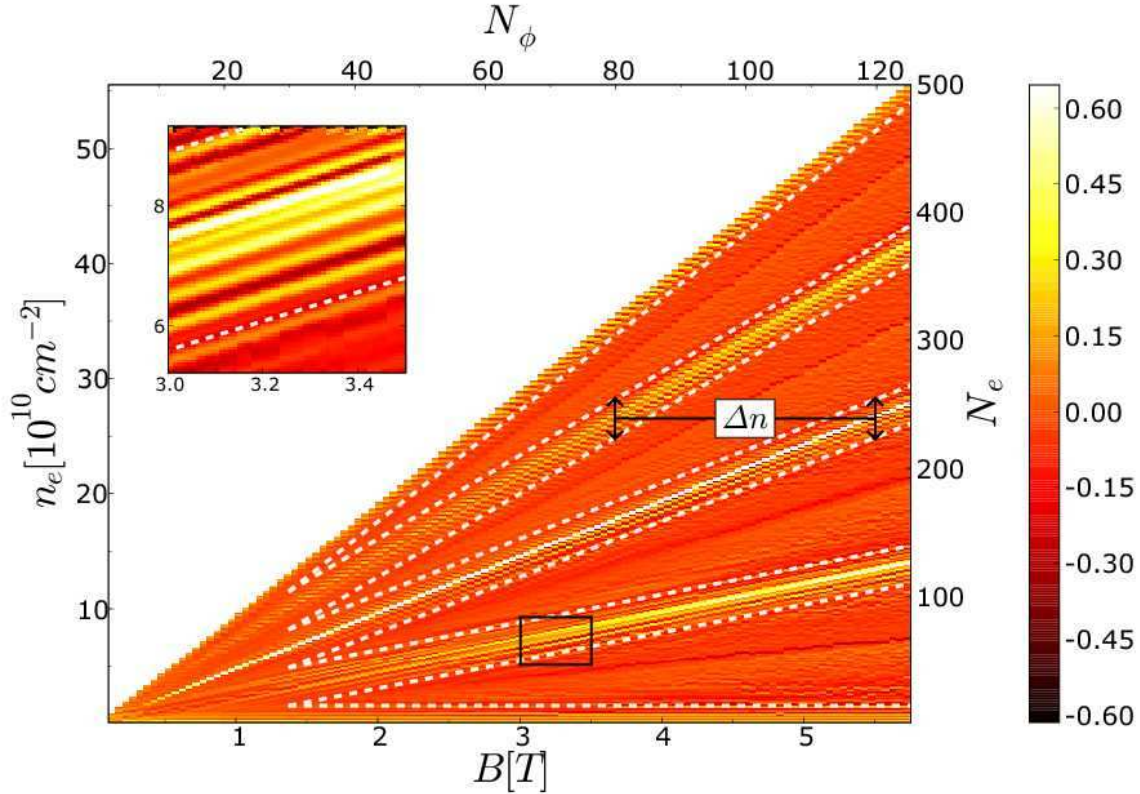
Figure 5. Inverse electronic compressibility κ^{-1} for a HF-interacting system of size $L = 300$nm with disorder strength $W/d^2 = 1.25$meV in the (B, n_e)-plane. The dotted lines show estimates based on a perfect screening condition (see text for details). The color scale spans two standard deviations around the average of κ^{-1}. The inset shows more detailed results for the region marked by a black rectangle.

to the effects observed in the experiments of [16, 17]. Outside the stripes, there is hardly any feature in the compressibilities except directly at the QH plateau-to-plateau transitions at half-integer fillings where a small increase in compressibility is discernible. In these areas between incompressible stripes, the inverse compressibility tends to have a very low or even negative value, which relates to a very high or negative TDOS, respectively. This effect has been observed experimentally [61, 62] and is a signature of the exchange interaction. From the proportionality between compressibility and the screening length, we can conclude to observe strong overscreening in the areas of negative compressibility. We attribute this to the tendency of the HF-interacting 2DES to form a charge density wave [35, 63]. Furthermore, when comparing Figures 5, 6, and 7 we find that the width of the incompressible stripes increases with increasing disorder strength W/d^2.
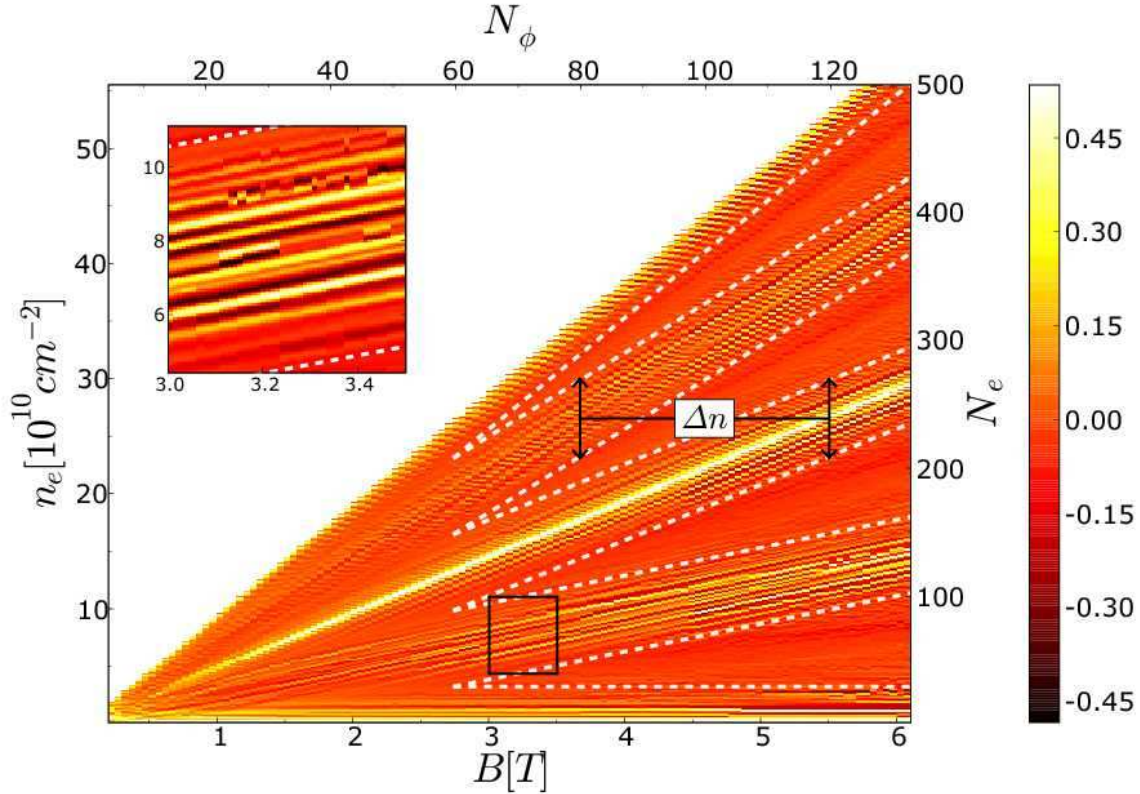
Figure 6. Inverse electronic compressibility as in Figure 5 but with $W/d^2 = 2.5$meV.

8. Spatial distribution of electronic density and screening

The spatial distribution of the total electronic density

$$n(\vec{r}) = \sum_{\sigma} \sum_{\alpha=1}^{M} |\psi_{\alpha}^{\sigma}(\vec{r})|^2 \tag{18}$$

$$= L^{-2} \sum_{\sigma} \sum_{n,k,n',k'} \sum_{\vec{q}} \mathbf{D}_{n,k;n',k'}^{\sigma} S_{n,k;n',k'}(\vec{q}) \exp(-i\vec{q}\vec{r}) \tag{19}$$

is readily calculated in our model. It details the screening mechanism by providing direct insight into the interplay of disorder and interaction. Let us start at the QH transition. Figure 8 depicts the critical charge density at $\nu = 1/2$ for a non-interacting system in units of n_0. The contour lines show the impurity potential $V_I(\vec{r})$ where the critical energy $V_I(\vec{r}) = \epsilon_F$ is highlighted by a thick line. The charge density evidently behaves according to the semiclassical approximation [23] and follows the equipotential lines of $V_I(\vec{r})$. For the interacting case, however, we expect Thomas-Fermi screening theory to apply [64–67]. The electrostatic potential of the charge density

$$\phi(\vec{r}) = \frac{e}{4\pi\epsilon\epsilon_0} \int d^2\vec{r}' \frac{n(\vec{r}') - \bar{n}}{|\vec{r}' - \vec{r}|} \tag{20}$$

and the impurity potential $V_I(\vec{r})$ form a screened potential $V_{scr}(\vec{r}) = V_I(\vec{r}) + e\phi(\vec{r})$. Here, $\bar{n}$ accounts for the positive background. Since a flat screened potential is energetically
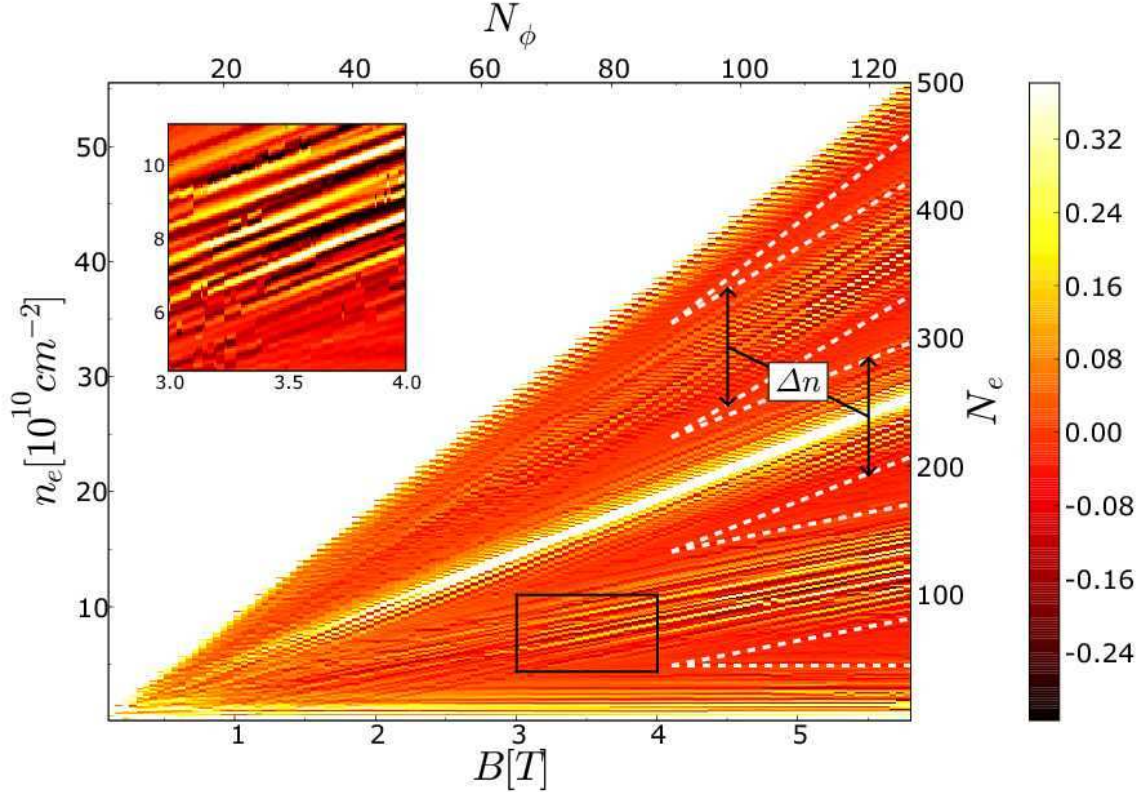
Figure 7. Inverse electronic compressibility as in Figure 5 but with $W/d^2 = 3.75$meV.

most favourable, one expects to find $V_{\mathrm{scr}}(\vec{r}) = \epsilon_{\mathrm{F}}$ for the case of perfect screening. However, since fluctuations of the density, $\delta n(\vec{r}) = n(\vec{r}) - \bar{n}$, are restricted between an empty and a full Landau level, i.e. $0 < \delta n(\vec{r}) < n_0$, the screening is not always perfect but depends on the fluctuations in the impurity potential as well as on the filling factor [64–66]. The plane can be divided into fully electron or hole depleted, insulating regions — where $n(\vec{r}) = 0$ or $n(\vec{r}) = n_0$, respectively — and metallic regions — where $n(\vec{r})$ lies in between. Depending on the filling factor, the extent of those regions varies. Close to the band edge, insulating regions dominate. Screening is highly non-linear and transport virtually impossible. On the other hand, if disorder is weak enough, there exists a finite range of filling factors in the centres of each band where metallic regions cover most of the sample, percolate and render the whole system metallic. The disorder is effectively screened and transport greatly enhanced. In that case, the charge density $n_{\mathrm{scr}}(\vec{r})$ can be obtained by Fourier transforming the screened potential. In 3D, this simply leads to the Laplace equation. For 2D, however, one obtains [68]

$$n_{\mathrm{scr}}(\vec{q}) = -\frac{2\epsilon\epsilon_0}{e^2}|\vec{q}|V_{\mathrm{I}}(\vec{q}) + \nu n_0\delta_{q,0}, \tag{21}$$

where the $|\vec{q}| = 0$ term is "perfectly screened" by the positive background and thus does not contribute to screening of the impurity potential. In other words, in our model only the fluctuations $\delta n(\vec{r})$ are essential for screening. Hence, in 2D, a perfectly screening
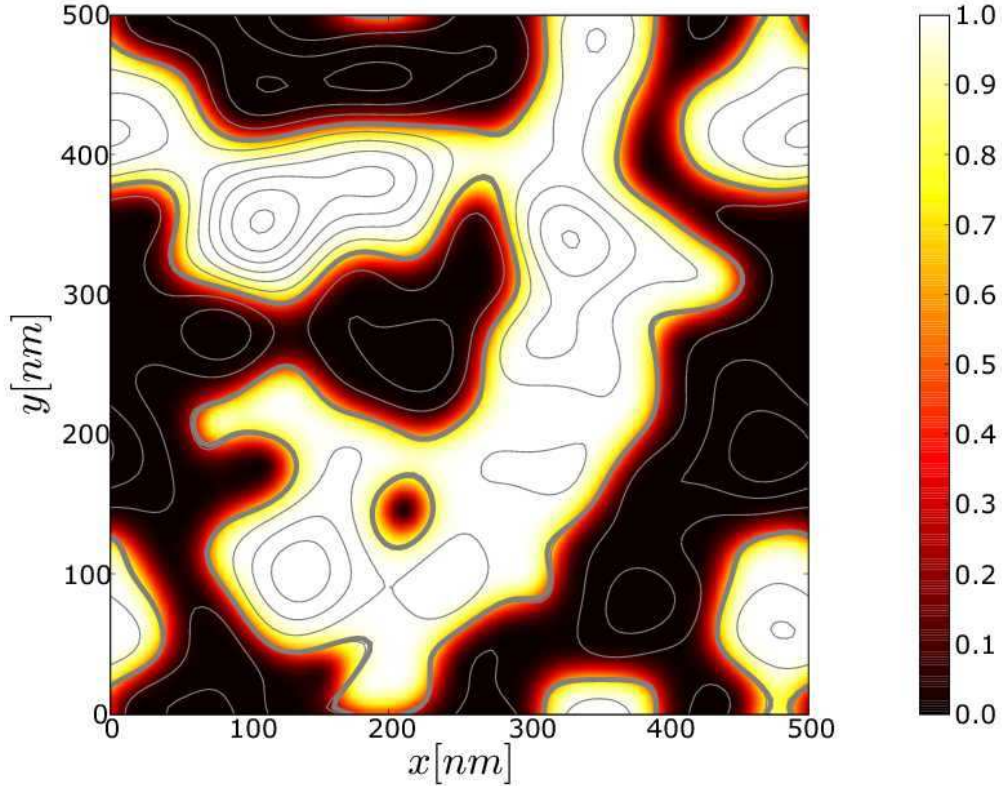
Figure 8. Spatial distribution of non-interacting electron density $n(\vec{r})/n_0$ at $B = 4\text{T}$, $\gamma = 0$ and $\nu = 1/2$ as indicated by the color scale. Solid contour lines show the equipotential lines of the $V_\text{I}(\vec{r})$. The thick solid lines corresponds to ϵ_F.

charge density would obey

$$n_\text{scr}(\vec{r}) = -\frac{4\pi\epsilon\epsilon_0}{e^2} \int d^2\vec{r}' \frac{\Delta_\text{2D}V_\text{I}(\vec{r}')}{|\vec{r} - \vec{r}'|} + \nu n_0. \tag{22}$$

Clearly, the actual charge density is expected to deviate from $n_\text{scr}(\vec{r})$ for several reasons. Firstly, the fluctuations of $n(\vec{r})$ are restricted as discussed above. Secondly, (22) is valid for the Hartree case only. Taking the Fock contribution into account will introduce short wavelength fluctuations due to the tendency for crystalization. However, we still expect the charge density to follow (22) in the limit of $|\vec{q}| \to 0$ [69]. Figure 9 shows results for the charge density of interacting electrons at $\nu = 1/2$. Broken lines indicate the regions where $n_\text{scr}(\vec{r})$ exceeds the range for $\delta n(\vec{r})$ either below or above, i.e. areas that cannot be screened at all and thus exhibit insulating behaviour. Otherwise, we find the charge density to follow $n_\text{scr}(\vec{r})$ very closely. In this regime, the density is well described by (22) and the screening is very effective. Metallic regions dominate over insulating ones and transport is expected to be good. In Figure 10 we depict cross-sectional plots of $n(\vec{r})$ and $n_\text{scr}(\vec{r})$ for the sample of Figure 9 at $x = 100\text{nm}$ and three different filling factors, demonstrating the discussed effects again very clearly.
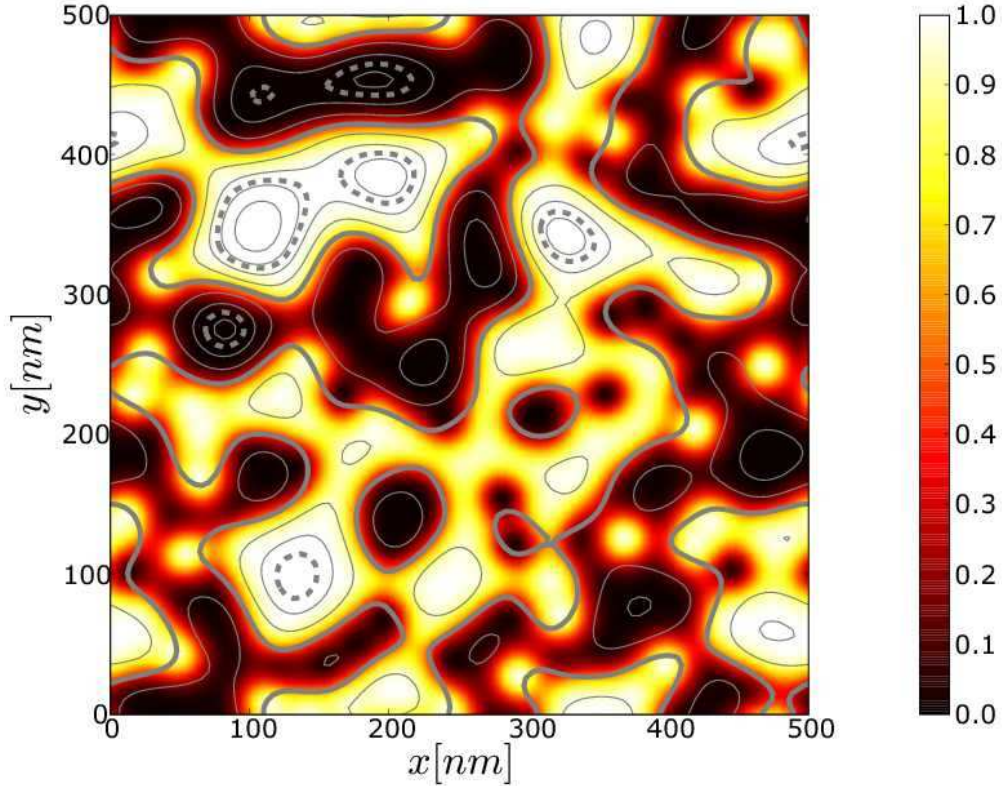
Figure 9. Spatial distribution of HF-interacting electron density $n(\vec{r})/n_0$ at $B = 4\mathrm{T}$, $\gamma = 0.3$ and $\nu = 1/2$ as indicated by the color scale. Contour lines show (21). The broken lines indicate unscreenable (insulating) regions. The thick solid line shows $n_{\mathrm{scr}}(\vec{r}) = \bar{n}_{\mathrm{scr}} = 0$.

9. Breakdown of linear screening

Thus far we have shown that our results can qualitatively reproduce the structures observed in the (B, n_{e}) plots of the compressibility. We find stripes of constant width with very similar characteristics as in the experiments. Furthermore, we show that within HF, the impurity potential in the band centre can be quite effectively screened by the charge density. Let us now turn our attention to the stripes. The screening of the impurity potential is non-linear near the edges of the Landau bands. Most of the sample is thus covered by insulating regions where the Landau band is either completely depleted or filled. Metallic behaviour is confined to small regions around potential extrema, where electron or hole islands are formed. If additional charge is introduced into the system, charging effects will govern the spectrum. These charging effects will manifest themselves in jumps in the compressibility as a function of charge density. The simple dot model of [28] was able to account for this effect and even demonstrated that charging events will take place along lines of integer filling factor, in agreement with our calculations. An estimation for the cross-over from linear to non-linear screening can be found by very general considerations [70]. An insulating island where $n(\vec{r}) = n_0$ is
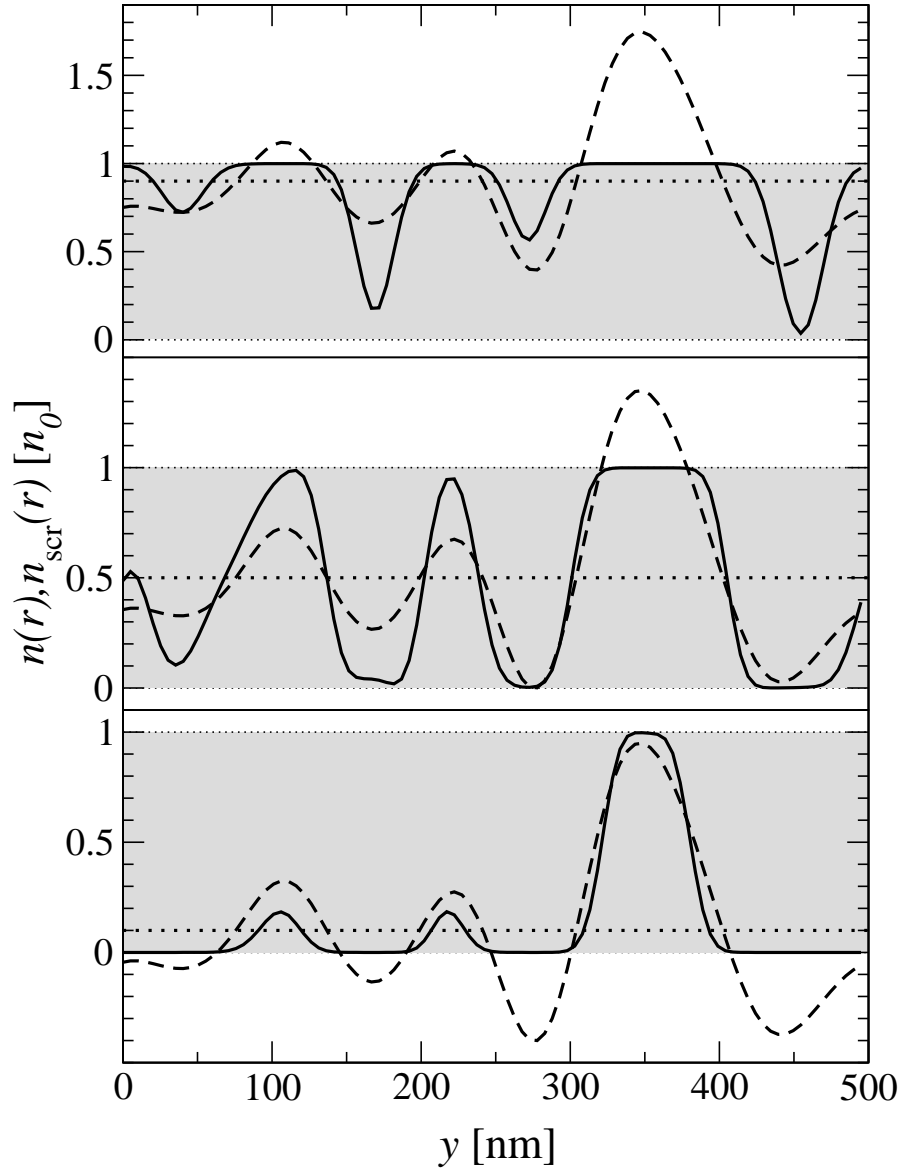
Figure 10. Cross-sections of the system of Figure 9 at $x = 100$nm and filling factors $\nu = 0.1$, $\nu = 0.5$, and $\nu = 0.9$ (bottom to top). Full curves correspond to $n(\vec{r})$, broken lines show (22). A thick horizontal dotted line shows the average charge density, νn_0. The grey areas, bounded by thin dotted lines, indicate the complete band.

confined by the force of the impurity potential, $\nabla V_{\mathrm{I}}(\vec{r})$, around its edge. Thereby, the Coulomb interactions opposing this force making the edge of the full region metallic. The size of the edges, i.e. the size of the metallic region, is then determined by the Coulomb force $n_0 e^2 / 2\pi\epsilon\epsilon_0$. Only if the Coulomb force acquires a magnitude comparable to the typical confining potential force, the metallic edges of the full islands will connect and dominate over the insulating regions. The typical force of our impurity potential is given by $\langle |\nabla V_{\mathrm{I}}(\vec{r})|^2 \rangle = n_{\mathrm{I}} \langle w_s{}^2 \rangle_s / \pi d^4$. We would like to remark that with $N_{\mathrm{I}} = 288$, the expected standard deviation of $\langle w_s{}^2 \rangle_s$ is $\sim 2\%$, which makes the typical force a reliable characteristic of V_{I} for finite sample calculations. From equating the typical force with
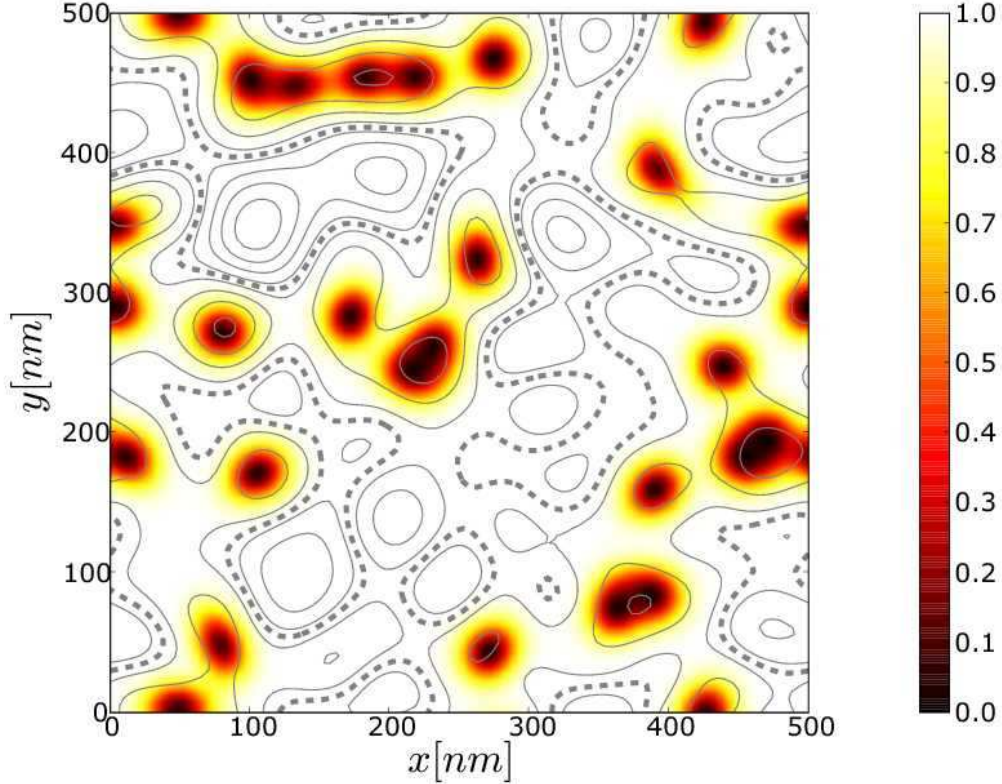
Figure 11. Spatial distribution of HF-interacting electron density $n(\vec{r})/n_0$ at $B = 4\mathrm{T}$, $\gamma = 0.3$ and $\nu = 0.9$ as indicated by a color scale. Solid contour lines show the equipotential lines of (21). The broken lines indicate unscreenable (insulating) regions.

the Coulomb force we can derive an expression for the minimal required density n_0 which corresponds to a minimum magnetic field $B_{\min} = n_0 h/e$ below which linear screening breaks down for any density. Therefore, n_0 determines the width of the charging stripes Δn and we find

$$\Delta n = n_0 = \frac{2\pi\epsilon\epsilon_0}{\gamma e^2}\sqrt{\langle|\nabla V_{\mathrm{I}}(\vec{r})|^2\rangle} = \frac{2\pi\epsilon\epsilon_0}{\gamma e^2}\sqrt{\frac{n_{\mathrm{I}}}{3\pi}}\frac{W}{d^2}. \tag{23}$$

Note that Δn is indeed independent of B and n_{e} as observed in the experiments. In Figures 5, 6, and 7, we have indicated the breakdown of the linear screening regime by dashed white lines. The points at which the lines merge indicate $B_{\min}$. Evidently, (23) nicely estimates the widths of the observed stripes for all three disorder configurations used. Furthermore, we have tested the criterion for breakdown by plotting compressibilities as a function of n_{e} and disorder strength W/d^2. Figure 12 shows the result for W/d^2 between 1meV and 3meV at $B = 3.5\mathrm{T}$. The dashed white lines again indicate (23). In order to confirm the dependence of the stripes on the ratio between W and d^2 only, the plot has been divided into two regimes. Between 1meV and 2meV, we kept $d = 40\mathrm{nm}$ as a constant and varied W, and between 2meV and 3meV we kept $W/\mathrm{nm}^2 = 3.2\mathrm{meV}$ constant whilst varying d, accordingly. The results confirm (23). Deviations from the expected behaviour can be explained with the proximity to the

disorder dominated regime for higher values of W/d^2 where $B \simeq B_{\min}$. This regime is strongly disorder dominated and charging effects become much less pronounced at the band edges.
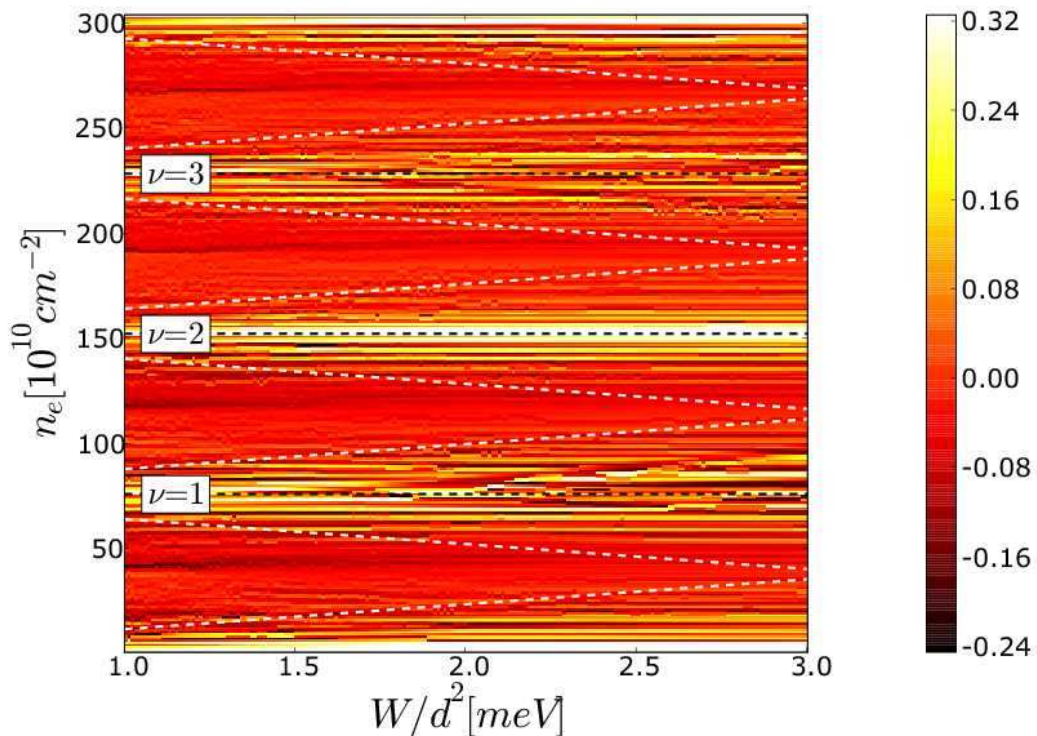

Figure 12. Inverse electronic compressibility κ^{-1} for a HF-interacting system ($\gamma = 0.3$) of size $L = 300$nm in the $(W/d^2, n_e)$-plane. Dashed white lines indicate expected boundaries of linear screening as calculated from (23), dashed black lines show integer filling factors.

10. Conclusions

We have investigated numerically how electron-electron interactions affect the localization properties of a 2DES under influence of a strong perpendicular magnetic field. We therefore diagonalized the Hamiltonian in a suitable basis and treated interactions as an effective mean field.

Our calculations reveal substantial differences in the electronic compressibility between non-interacting and interacting systems when viewed as a function of magnetic field and carrier density. For interacting systems, we find strongly incompressible stripes of constant width around integer filling factors. We show the dependence of the width of the stripes on the disorder configuration and compute the width based on a force balance argument. These results are in very good agreement with recent imaging experiments. Moreover, we find strong g-factor enhancement as well as negative compressibility in the

band centres, also consistent with experiments. We demonstrate that the incompressible patterns can be attributed to non-linear screening effects in the tails of the Landau bands. For magnetic fields larger than $B_{\min}$, the effects of linear screening — and hence interactions — dominate in the (B, n_{e})-plane. Thus, our results support the existence of a greater variety of transport regimes due to electron-electron interactions in the integer quantum Hall effect.

Similar compressibility patterns have also been observed around fractional filling factors $\nu = 1/3, 2/5$, and $2/3$ [17]. Energy gaps at fractional filling, e.g. $\nu = p/(2p+1)$, with p being an integer, are a consequence of electron correlations which are absent in HF approximation. However, with the formal analogy [71] between IQHE and FQHE put forward by the composite fermion (CF) model [72, 73], let us venture a few statements about compressibility patterns around those fractional fillings. It is argued that the FQHE can be regarded as a manifestation of the IQHE for CFs in an effective magnetic field $B^* = B_\nu - B_{\nu=1/2}$ [74, 75]. If we pretend to have obtained results for CFs in an (B^*, n_{CF}) plane, a transformation back to electrons yields an increase in the density of charging lines (per n_{e}) by a factor of $2p+1$. Indeed, in the above mentioned experiment an increase of 3 has been found for $\nu = 1/3$. Furthermore, such a transformation predicts a dependence of the width of the incompressible stripes on the filling factor as well as a strong increase of $B_{\min}$ when fractional filling factors approach $\nu = 1/2$. This remains yet to be explored.

Acknowledgements

Appendix A. Plane wave matrix elements and boundary conditions

For $n \geq m$, the plane wave matrix elements $S_{n,k;n',k'}(\vec{q})$ read

$$\langle nk| \exp(i\vec{q} \cdot \vec{r})|mj\rangle = \delta'_{q_y,k-j} \sqrt{\frac{2^n m!}{2^m n!}} e^{-\frac{\vec{q}^2}{4} + \frac{i}{2} q_x(k+j)} \left(\frac{iq_x - q_y}{2}\right)^{n-m} L_m^{n-m}\left(\frac{\vec{q}^2}{2}\right), \quad \text{(A.1)}$$

where $L_n^a(x)$ is the generalized Laguerre polynomial. For periodic boundaries, the delta function is defined with modulus, i.e.

$$\delta'_{a,b} = \begin{cases} 1 & \text{if} \quad \mathrm{mod}(a-b, N_\phi) = 0, \\ 0 & \text{otherwise.} \end{cases} \quad \text{(A.2)}$$

The periodic boundary conditions require careful treatment of the overlap between Landau functions at opposite sites of the sample. We only take $|mj\rangle$ to be a replicated Landau function in one unit cell to the right and one to the left of the sample, whereas $\langle nk|$ remains in the base cell. A check of the implementation can be carried out by noting that a shift of the impurities by L/N_ϕ along the x or the y direction should only shift the wave-functions, $\psi_\alpha^\sigma(\vec{r})$, by the same value. Finally we would like to remark that the complexity of summations involving plane wave matrix elements can be greatly reduced by neglecting terms where $\exp(-\vec{q}^2/2) < \varepsilon$. One can apply the restriction $|q_x|^2 < \max(0, -2\ln(\epsilon) - q_y^2)$ to summations over q_x, usually leading to a substantial reduction of complexity even for $\varepsilon \sim 10^{-10}$.

Appendix B. Bielectronic integrals

Summations containing the bielectronic integrals

$$G_{n,k;n',k'}^{m,l;m',l'} = \sum_{\vec{q}\neq 0} v(\vec{q}) S_{n,k;n',k'}(\vec{q}) S_{m,l;m',l'}(-\vec{q}) \tag{B.1}$$

can be substantially simplified by virtue of the delta function (A.2) contained in the plane wave matrix elements. Ultimately, two of the summations in (8) drop out. We can replace q_y by $k - k'$ and l' by $l + k - k'$, and if $n \geq m$ as well as $n' \geq m'$, we get

$$G_{n,k;n',k'}^{m,l;m',l'} = \delta_{q_y,k-k'}\delta_{l',l+k-k'} \sum_{q_x} v(\vec{q})\sqrt{\frac{2^{n_a}n_b!}{2^{n_b}n_a!}}\sqrt{\frac{2^{n_c}n_d!}{2^{n_d}n_c!}}e^{-\frac{\vec{q}^2}{2}+iq_x(k'-l)} \times \tag{B.2}$$

$$\times \left(\frac{iq_x - q_y}{2}\right)^{n_a-n_b} \left(\frac{-iq_x + q_y}{2}\right)^{n_c-n_d} L_{n_b}^{n_a-n_b}\left(\frac{\vec{q}^2}{2}\right) L_{n_d}^{n_c-n_d}\left(\frac{\vec{q}^2}{2}\right). \tag{B.3}$$

[1] K. v. Klitzing, G. Dorda, and M. Pepper, Phys. Rev. Lett. **45**, 494 (1980).
[2] R. E. Prange, Phys. Rev. B **23**, 4802 (1981).
[3] T. Chakraborty and P. Pietilänen, *The Quantum Hall effects* (Springer, Berlin, 1995).
[4] M. Janssen, O. Viehweger, U. Fastenrath, and J. Hajdu, *Introduction to the Theory of the Integer Quantum Hall effect* (VCH, Weinheim, 1994).
[5] R. B. Laughlin, Phys. Rev. B **23**, 5632 (1981).
[6] A. M. M. Pruisken, Nucl. Phys. B **235**, 277 (1984).
[7] D. J. Thouless, M. Kohmoto, M. P. Nightingale, and M. den Nijs, Phys. Rev. Lett. **49**, 405 (1982).
[8] A. M. M. Pruisken, in *The Quantum Hall Effect*, edited by R. E. Prange and S. M. Girvin (Springer, Berlin, 1987).
[9] J. T. Chalker and P. D. Coddington, J. Phys.: Condens. Matter **21**, 2665 (1988).
[10] P. Cain and R. A. Römer, EuroPhys. Lett. **66**, 104 (2004).
[11] B. Kramer, T. Ohtsuki, and S. Kettemann, Phys. Rep. **417**, 211 (2005), ArXiv: cond-mat/0409625.
[12] B. Huckestein and B. Kramer, Phys. Rev. Lett. **64**, 1437 (1990).
[13] S. Koch, R. J. Haug, K. v. Klitzing, and K. Ploog, Phys. Rev. Lett. **67**, 883 (1991).
[14] K. v. Klitzing and G. Ebert, Metrologia **21**, 11 (1985).
[15] D. H. Cobden, C. H. W. Barnes, and C. J. B. Ford, Phys. Rev. Lett. **82**, 4695 (1999).
[16] S. Ilani *et al.*, Nature **427**, 328 (2004).
[17] J. Martin *et al.*, Science **305**, 980 (2004).
[18] D. Shahar *et al.*, Solid State Commun. **107**, 19 (1998), ArXiv: cond-mat/9706045.
[19] N. Q. Balaban, U. Meirav, and I. Bar-Jospeh, Phys. Rev. Lett. **81**, 4967 (1998).
[20] H. Aoki and T. Ando, Phys. Rev. Lett. **54**, 831 (1985).

[21] J. T. Chalker and G. J. Daniell, Phys. Rev. Lett. **61**, 593 (1988).
[22] D. Liu and S. Das Sarma, Phys. Rev. B **49**, 2677 (1994).
[23] B. Huckestein, Rev. Mod. Phys. **67**, 357396 (1995).
[24] J. Sinova, V. Meden, and S. M. Girvin, Phys. Rev. B **62**, 2008 (2000), ArXiv: cond-mat/0002202.
[25] P. Cain and R. A. Römer, Int. J. Mod. Phys. B **19**, 2085 (2005).
[26] C. Sohrmann and R. A. Römer, phys. stat. sol. (b) **3**, 313 (2005).
[27] A. Struck and B. Kramer, Phys. Rev. Lett. **97**, 106801 (2006).
[28] A. Pereira and J. Chalker, (2005), arXiv: cond-mat/0502304.
[29] D.-H. Lee and Z. Wang, Phys. Rev. Lett. **76**, 4014 (1996).
[30] S.-R. E. Yang, A. H. MacDonald, and B. Huckestein, Phys. Rev. Lett. **74**, 3229 (1995).
[31] D. Yoshioka, B. I. Halperin, and P. A. Lee, Phys. Rev. Lett. **50**, 1219 (1983).
[32] L. D. Landau and E. M. Lifshitz, *Quantum Mechanics* (Butterworth-Heinemann, Oxford, 1981).
[33] H. Aoki, J. Phys. C **12**, 633 (1979).
[34] A. H. MacDonald and G. C. Aers, Phys. Rev. B **34**, 2906 (1986).
[35] D. Yoshioka and H. Fukuyama, J. Phys. Soc. Jpn. **47**, 394 (1979).
[36] A. MacDonald and S. Girvin, Phys. Rev. B **38**, 6295 (1988).
[37] M. Backhaus and B. Huckestein, World Scientific. Physics B **15**, 1369 (2001).
[38] C. C. J. Roothaan, Rev. Mod. Phys. **23**, 69 (1951).
[39] In (11) we have omitted the overlap matrix for the molecular orbitals, which is simply the unity matrix for our Landau functions.
[40] E. Cancès and C. L. Bris, Int. J. Quantum Chem. **79**, 82 (2000).
[41] V. R. Saunders and I. H. Hillier, Int. J. Quantum Chem. **7**, 699 (1973).
[42] G. D. Mahan, *Many Particle Physics* (Kluwer Academic/Plenum, New York, 2000).
[43] J. K. Jain and S. A. Kivelson, Phys. Rev. Lett. **60**, 1542 (1988).
[44] N. W. Ashcroft and N. D. Mermin, *Solid State Physics* (Saunders College, New York, 1976).
[45] T. Ando, A. B. Fowler, and F. Stern, Rev. Mod. Phys. **54**, 437 (1982).
[46] S. Das Sarma and F. Stern, Phys. Rev. B **32**, 8442 (1985).
[47] When more realisticly Coulomb interaction between electrons and impurities is assumed, a logarithmic dependence on the sample size is found [64].
[48] S.-R. E. Yang and A. H. MacDonald, Phys. Rev. Lett. **70**, 4110 (1993).
[49] H. Aoki, J. Phys. C **16**, L205 (1983).
[50] H. Aoki, Phys. Rev. B **33**, 7310 (1986).
[51] We emphasize that a proper use of participation numbers should not simply compare their values for different states at fixed system size as this can lead to wrong conclusions. Rather, their system size dependence must be studied [52].
[52] A. Eilmes, R. A. Römer, and M. Schreiber, Eur. Phys. J. B **1**, 29 (1998).
[53] M. Backhaus and B. Huckestein, Physica B **256–58**, 52 (1998).
[54] J. Bauer, T.-M. Chang, and J. L. Skinner, Phys. Rev. B **42**, 8121 (1990).
[55] C. M. Soukoulis and E. N. Economou, Phys. Rev. Lett. **52**, 565 (1984).
[56] M. Janssen, Int. J. Mod. Phys. B **8**, 943 (1994).
[57] B. Huckestein and L. Schweitzer, Phys. Rev. Lett. **72**, 713 (1994).
[58] J. F. Janak, Phys. Rev. **178**, 1416 (1969).
[59] R. J. Nicholas, R. J. Haug, K. v. Klitzing, and G. Weimann, Phys. Rev. B **37**, 1294 (1988).
[60] A. Manolescu and R. R. Gerhardts, Phys. Rev. B **51**, 1703 (1995).
[61] S. V. Kravchenko, V. M. Pudalov, and S. G. Semenchinsky, Physics Letters A **141**, 71 (1989).
[62] J. P. Eisenstein, L. N. Pfeiffer, and K. W. West, Phys. Rev. Lett. **68**, 674 (1992).
[63] R. Côté and A. H. MacDonald, Phys. Rev. B **44**, 8759 (1991).
[64] A. L. Efros, J. Comput. System Sci. **65**, 1281 (1988).
[65] A. L. Efros, Solid State Commun. **67**, 1019 (1988).
[66] A. L. Efros, Solid State Commun. **70**, 253 (1989).
[67] A. L. Efros, Phys. Rev. B **45**, 11354 (1992).

[68] U. Wulf, V. Gudmundsson, and R. R. Gerhardts, Phys. Rev. B **38**, 4218 (1988).

[69] Note that the matrix $\tilde{\mathbf{H}} \equiv \mathbf{V} + \mathbf{F}_{\text{Hartree}}$, i.e. including only the disorder and Hartree terms, is simply $V_{\text{scr}}(\vec{r})$ in the Landau basis. Thus an operation such as $\text{Tr}(\tilde{\mathbf{H}}\tilde{\mathbf{H}}^*)$ can be regarded as a measure for how well the disorder is screened [76].

[70] N. R. Cooper and J. T. Chalker, Phys. Rev. B **48**, 4530 (1993).

[71] J. K. Jain, Physica E **20**, 79 (2003).

[72] J. K. Jain, Phys. Rev. Lett. **63**, 199 (1989).

[73] J. K. Jain, Physics Today 39 (2000).

[74] R. R. Du *et al.*, Phys. Rev. Lett. **70**, 2944 (1993).

[75] H. L. Stormer, D. C. Tsui, and A. C. Gossard, Rev. Mod. Phys. **71**, S298 (1999).

[76] C. Sohrmann, Ph.D. thesis, University of Warwick, 2007, in preperation.